sensors

Article

Correction of Radiometry Data for Temperature Effect on Dark Current, with Application to Radiometers on Profiling Floats

Terence O'Brien [1,*] and Emmanuel Boss [2]

[1] Institute for the Study of Earth, Ocean and Space, University of New Hampshire, Durham, NH 03824, USA
[2] School of Marine Sciences, University of Maine, Orono, ME 04469, USA
[*] Correspondence: terence.obrien@unh.edu

Abstract: Measurements of daytime radiometry in the ocean are necessary to constrain processes such as photosynthesis, photo-chemistry and radiative heating. Profiles of downwelling irradiance provide a means to compute the concentration of a variety of in-water constituents. However, radiometers record a non-negligible signal when no light is available, and this signal is temperature dependent (called the dark current). Here, we devise and evaluate two consistent methods for correction of BGC-Argo radiometry measurements for dark current: one based on measurements during the day, the other based on night measurements. A daytime data correction is needed because some floats never measure at night. The corrections are based on modeling the temperature of the radiometer and show an average bias in the measured value of nearly 1×10^{-4} W m^{-2} nm^{-1}, an order of magnitude larger than the reported uncertainty of 2.5×10^{-5} W m^{-2} nm^{-1} for the sensors deployed on BGC-Argo floats (SeaBird scientific OCR504 radiometers). The methods are designed to be simple and robust, requiring pressure, temperature and irradiance data. The correction based on nighttime profiles is recommended as the primary method as it captures dark measurements with the largest dynamic range of temperature. Surprisingly, more than 28% of daytime profiles (130,674 in total) were found to record significant downwelling irradiance at 240–250 dbar. The correction is shown to be small relative to near-surface radiance and thus most useful for studies investigating light fields in the twilight zone and the impacts of radiance on deep organisms. Based on these findings, we recommend that BGC-Argo floats profile occasionally at night and to depths greater than 250 dbar. We provide codes to perform the dark corrections.

Keywords: radiometry; Argo floats; dark corrections

check for updates

Citation: O'Brien, T.; Boss, E. Correction of Radiometry Data for Temperature Effect on Dark Current, with Application to Radiometers on Profiling Floats. *Sensors* **2022**, *22*, 6771. https://doi.org/10.3390/s22186771

Academic Editor: Flavio Esposito

Received: 29 July 2022
Accepted: 1 September 2022
Published: 7 September 2022
Corrected: 19 June 2023

1. Introduction

Sunlight fuels primary production in the oceans through microbial photosynthesis and is the primary source of thermal energy to the upper ocean. Accurate estimates of global primary production, oceanic photo-oxidation and thermal transfer are essential for quantifying both ocean carbon capture and long-term carbon storage in the deep ocean, as well as for providing radiative forcing for oceanographic and meteorological models. Downwelling planar irradiance, E_d, throughout the water column is one of the fundamental optical measurements from which the diffuse attenuation coefficient, K_d [m^{-1}], an apparent optical property, is derived. Additionally, vertical profiles of the spectral diffuse attenuation allow important water constituents such as chlorophyll and colored dissolved organic concentrations to be estimated [1,2].

The Argo program is a global array of profiling floats funded by national agencies. Since its first deployment in 1999, the array of Argo floats has grown to nearly 4000. These profile from the surface to 2000 dbar every 10 days, collecting CTD data. The project has expanded into Biogeochemical (BGC)-Argo by including optical, oxygen, nitrate and pH sensors on some floats [3]. Because the floats experience a dramatic range of temperature and pressure, and the sensors are not calibrated after deployment, it is essential to investigate the dynamics of sensor behavior. Without the retrieval of the sensors post-deployment, this must be done through investigation of the collected data.

Radiometers report a non-negligible output, known as the 'dark current', even in the complete absence of ambient light. Furthermore, this dark current is known to display a temperature dependence. This is the reason why some commercial radiometers (e.g., SeaBird's Hyper-OCR) have shutters allowing dark measurements to be taken in between readings of ambient light. SeaBird's OCR504 radiometers, however, which are installed on the majority of BGC-Argo floats, do not have shutters (shutters increase energy consumption and cost). These radiometers have been shown to have a temperature-dependent dark response up to 2 or more times the known sensitivity of 2.5 $\times$ 10^{-5} W m^{-2} nm^{-1} for E_d (380 nm, 412 nm, 490 nm) [4,5]. These sensors have an additional channel measuring the intensity of photosynthetically available radiation (PAR), which has also been found to exhibit a temperature-dependent dark response [4,5]. To accurately characterize oceanographic processes at depth or in low-light conditions, where uncertainties in the radiometric measurements may be significantly impacted by uncertainties in the blank, a correct calibration which includes a correction for the temperature-sensitive dark current is essential [4,6]. Here, we investigate the dependence of the dark measurements (where measured irradiance is expected to be zero) on sensor temperature T_s for radiometers on BGC-Argo floats and provide a quality control (QC) framework for correcting radiometer dark measurements for the instrument temperature dependence dE_{dark}/dT_s, [W m^{-2} nm^{-1} °C^{-1}] and $dPAR_{dark}/dT_s$, (µmol photons m^{-2} s^{-1} °C^{-1}) so that it can directly be applied by users. The analysis is done with data collected on floats characterized for this effect, which, as we show here, varies between individual radiometers in both magnitude and sign. We note that another paper with the same aims has been recently published, to which we have contributed [5]. However, the methods presented here are different and are intended to be applied directly to BGC-Argo s-files, rather than additionally using the Argo B- and transmission files (these contain data at float park depth, which we do not use here). Furthermore, unlike [5], we found no significant sensor drift over the lifetime of the floats analyzed once the temperature-dependent correction was applied.

2. Materials and Methods

Data from 218 BGC-Argo floats equipped with OCR504 radiometers, downloaded from https://www.ifremer.fr/erddap/tabledap/ArgoFloats.html (accessed on 28 March 2022), were investigated in this study. E_d at three wavelengths, 380 nm, 412 nm, and 490 nm (W m^{-2} nm^{-1}) and the instantaneous photosynthetically available radiation (iPAR, µmol photons m^{-2} s^{-1} from 400–700 nm) were used. The floats were located across the global ocean, samplng a range of conditions, from continental shelves to open ocean gyres and from high to low latitudes. Radiometers may sample every 10 meters from 1000 m to 250 m, though many record no radiometric measurements at all in this interval. Starting at 250 m, radiometric measurements are made every 1 m, and from 10 m to the surface every 0.2 m. The average number of profiles taken per float in this dataset was 200. The average number of "good" daytime radiometry profiles per float was ninety, as determined following QC procedures outlined in [7], namely taken during consistent wave and cloud conditions and with sun elevation above 15° to the horizon. The average number of nighttime profiles taken per float, defined as sun elevations below the horizon, was six. The average temperature range experienced by these floats over their lifetime during good radiometric profiles in this dataset was 12.44 °C.

With this dynamic temperature range and given that [4] showed the existence of a significant temperature response for these instruments, a temperature-dependent radiometric dark correction is necessary to accurately quantify or model processes occurring at low light levels. Sensor response to temperature varies between wavelengths for the same sensor and between sensors of the same model and may be positive or negative [4]. The response is dependent on sensor temperature rather than the ambient temperature (as expected for a temperature effect on the sensor electronics). We initially investigated the response based on ambient temperature, but found this inadequate as it exhibited a hysteresis, especially in regions with a pronounced thermocline. For this reason, a model of sensor temperature was developed similar to the one employed by [4].

Three approaches for quantifying temperature-dependent corrections for irradiance are investigated. Except where noted, the methods were identical for E_d and PAR. The first two involved calculating a robust least squares regression on dark values (where irradiance is evaluated to be zero within the noise of the instrument) for sensor temperature (T_s) vs. measured irradiance (E_d). This provided a linear equation for the dark values of the form:

$$E_d(dark, T_s) = x_0 + x_1 \times T_s, \tag{1}$$

where $x_1 = dE_d/dT_s$ and x_0 is a constant (equivalent to $E_d(dark, T_s = 0)$). The first method investigates night profiles, and the second investigates daytime profiles. The third method is designed to model the daytime profiles with a depth-dependent exponential + temperature dependent 1st degree polynomial. This further extended the range of depths where we could attempt to solve for the temperature sensitivity directly from daytime profiles. The model is:

$$E_d(z, T_s) = x_0 + x_1 \times T_s + x_2 \times \{exp(-x_3 \times (z - max(z))) - 1\}, \tag{2}$$

where x_0 is the predicted irradiance $E_d(dark, T_s = 0, z = max(z))$, x_1 is dE_d/dT_s, x_2 is a constant multiplier, and x_3 is the constant exponent for the depth-dependent (z is depth, positive downward) attenuation of irradiance. The model is fitted by the Levenberg–Marquardt method. While Equation (2) produced reasonable fits, the coefficients x_0 and x_1 showed a large range between profiles of the same float and, on average, had magnitudes significantly larger than those produced by Equation (1); they are thus assumed to represent a worse description of the temperature response of the sensor. We therefore decided not to use this model further.

Profile Extraction, Quality Control and Modeling

The QC procedures outlined in [7] were followed to flag BGC-Argo radiometry profiles with unreasonable measurements or profiles taken during inconsistent wave or cloud conditions. Night profiles were determined based on sun elevation being less than 0 degrees above horizon at the specified latitude, longitude and time (using the routine SolarAzEl.m [8]). The dark portion of daytime profiles, occurring at depths where no light is detected, were determined using a lilliefors test for normality outlined by [7].

To ensure that the "dark" profiles were not influenced by light, we deployed a test to distinguish sensor noise from low levels of irradiance (e.g., moon and star light) when the values of irradiance measured approached the uncertainty of the radiometer. At great depth, assuming the optical properties of the water are constant, we expect downwelling light to display monotonic exponential decay (thus a monotonic linear decay of log(E_d) with increasing depth) compared to random noise associated with the sensor. A least-squares regression of the depth (pressure) versus the log of the measured irradiance values was calculated for each profile. Any profile with a slope <-0.01 (log_{10} (W m^{-2} db^{-1})) and a Spearman's $\rho > 0.5$ (meaning the decrease is monotonic) is assumed to be measuring significant downwelling irradiance. Such a slope is indicative of a consistent decline in irradiance significantly larger than the reported sensor uncertainty (=2.5 $\times$ 10^{-5} W m^{-2} nm^{-1}).

For nighttime profiles that extend from $\sim$250 dbar to the surface, the test was applied three times to account for low levels of moonlight or starlight: from 150 dbar-surface, 100 dbar-surface, and 50 dbar-surface. For daytime profiles, the test was applied once, as the "dark" section generally spans a range of 10 m (240–250 dbar). For the daytime profiles (130,674 in total), 28% of "dark" profiles failed this test and were excluded from further analysis. For nighttime profiles (6281 in total), 51% fail at one of the depths (likely taken during twilight hours or under moonlight), with that section of the profile (from surface to given depth) removed from the regression analysis.

Following profile extraction, a model of the temperature-sensitivity of the dark current for each sensor was produced to correct for the effect of sensor temperature on the measured irradiance (dE_d/dT_s). We modeled the inherent lag in the sensor temperature by adjusting to that of the surrounding water column with a differential equation describing the relationship of the sensor temperature (T_s, unknown) to that of the water (T_{env}, measured by the float CTD sensor). The model is a first-order differential equation:

$$dT_s/dt = -(T_s - T_{env})/k \tag{3}$$

that has the explicit solution (see Appendix A):

$$T_s(t) = T_{env}(0)exp(\frac{-t}{k}) + exp(\frac{-t}{k}) \int_{t'=0}^{t'} \frac{exp(\frac{t'}{k}) \times T_{env}(t')}{k} dt, \tag{4}$$

where k is a time-lag constant. The rate of float rising was assumed to be constant with a value of 0.1 dbar/s [9]. We used k = 200 s (based on [4] and after finding no improvement upon exploring other values).

$T_s(t = 0)$, the initial condition of sensor temperature, was set to approximate the temperature of the sensor 20 m below $t = 0$ (thus 200 s previously), by calculating the average rate of change in the measured temperature (dT_{env}/dz) over the 20 m range 250–230 dbar and setting $T(t = 0) = T_{env}$ (250 dbar) $- dT_{env}/dz \times$ 20 m. This offset assumes a consistent gradient in temperature from 270–250 dbar and better models the temperature lag throughout the whole profile. If this resulted in a $T(t = 0)$ warmer than T_{env}(250 dbar), we required that $T(t = 0) = T_{env}$ (250 dbar). For profiles with measurements made below 250 dbar, where sampling frequency was inconsistent, $T(t = 0)$ was set to $T_{env}(t = 0)$, and data were linearly interpolated to a 1 dbar grid before the sensor temperature computation, with output only from sample depths saved.

A minimum/maximum range filter was applied to the irradiance profiles to remove remaining outlying values such as single spikes on otherwise good profiles, which may have been missed by previous filters. We constrained measurements to the range $|E_d| < 3 \times 10^{-4}$ W m^{-2} nm^{-1} and $|PAR| < 0.5$ µmol photons m^{-2} s^{-1}. These values were based on the distribution of measured irradiances from night profiles at depths greater than 300 dbar. In our dataset, 28% of nighttime values and 8% of daytime values were removed by this filter.

Following these QC steps, all the accepted profiles of a specific float and wavelength were compiled into a sensor-specific temperature versus irradiance database to determine a float-specific, wavelength-specific, temperature-dependent dark correction, which is assumed to be invariant in time. That is, the dark-current and temperature sensitivity were assumed constant throughout the life of a float, as we observed no evidence to the contrary. Daytime deep profiles and nighttime profiles were kept separate. The compiled profiles were then further subjected to the following two tests:

(a) Temperature range test: the temperature range of the compiled dark profiles must be greater than 2.5 °C. This test is important as the dE_d/dT_s is small (-3×10^{-5} to 3×10^{-5} W m^{-2} nm^{-1} °C^{-1}) and hence not detectable relative to other environmental processes if the temperature gradient in a profile is too small. Overall, 25% of night and 58% of day fits failed this test.

(b) Correlation test: Spearman's rank correlation coefficient (ρ) between irradiance and temperature must have an absolute value greater than 0.3. Spearman's tests how monotonic the relationship between two variables is (perfectly monotonic results in $|\rho = 1|$). This test determines if the signal of temperature is likely influencing the irradiance value. Too small a $|\rho|$ indicates it is likely undetectable in the available data. 13% of night and 17% of day data fits failed this test.

If both tests were satisfied, a robust linear fit (matlab robustfit.m) was computed from the compiled profiles of the specific float of sensor temperature (T_s) versus irradiance (E_d or PAR) to produce a float-specific, wavelength-specific dark offset correction (Equation (1)). A robust fit was used rather than a normal least-squares regression to reduce the weight of possible outliers in the profiles. Where one or both tests were not satisfied, the median $E_d(dark)$ of all floats was used for x_0 with $x_1 = 0$, (e.g., $dE_d/dT_s = 0$).

To ensure that we were not over-correcting for the temperature effect, we applied a filter based on the median (x_1) +/− 1.5 × IQR(x_1) across all models of the same wavelength to decrease outlying values of dE_d/dT_s. IQR is the interquartile range, the distance between the 25th and 75th percentiles. Because the sensors are all of similar make and model, we expected a bound on the maximum temperature dependence of the dark measurement. Corrections that fall outside of the upper and lower bounds of the median(x_1) +/− 1.5 × IQR(x_1) threshold had (x_1) set to the threshold bound (upper or lower). x_0 was adjusted so that dE_d/dT_s (x_1) intersects the median value of E_d (dark) for that float by specifying that x_0 = median(E_d) − x_1× median (E_d). A total of 8% of night profile values for x_1 and 2% of day profile values for x_1 were adjusted by this filter.

3. Results

Night profiles (method 1) and day profiles (method 2) produce comparable results for both correction parameters, x_0 (constant, [W m^{-2} nm^{-1}]) and x_1 (dE_d/dT_s, (W m^{-2} nm^{-1} °C^{-1})) (Equation (1), Figures 1 and 2). Method 1 is recommended as the primary correction as it samples from the larger temperature range (encompassing conditions encountered by floats during their full profiles), produces more non-zero x_1 values (Figure 1) and, on average, is a smaller correction (Table 1).

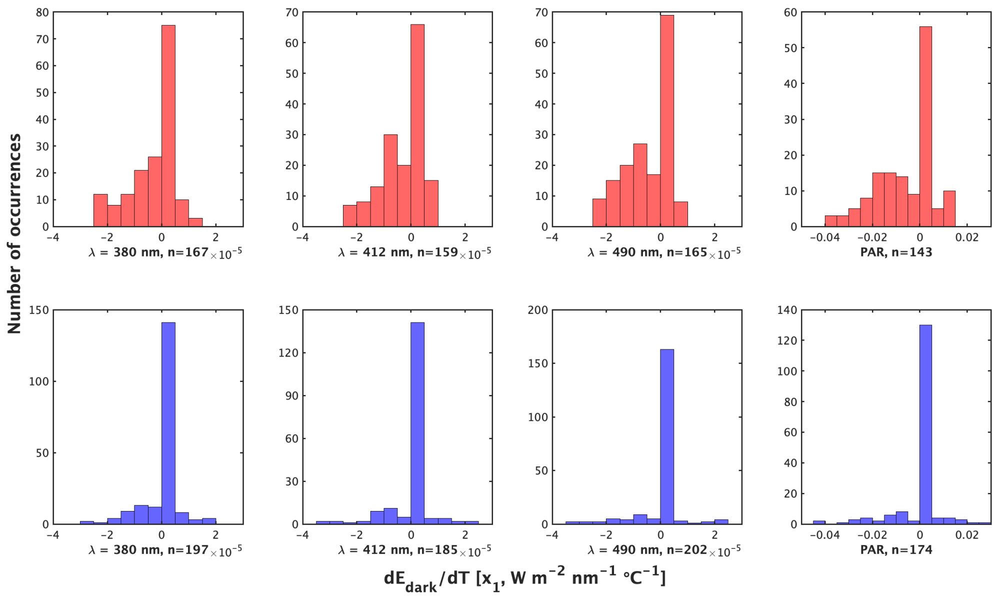

Figure 1. Histograms of the value of $x_1 = dE_d/dT_s$ (W m^{-2} nm^{-1}°C^{-1}) by the night method (**top**, red) and Day method (**bottom**, blue) for λ = 380 nm, 412 nm, 490 nm, and iPAR (**left** to **right**).

The median temperature range of compiled profiles by method 2 was 1.71 °C, with a median pressure range of 16.60 dbar. For comparison, the median temperature range of compiled nighttime profiles was 11.71 °C with a median pressure range of 250 dbar. The median temperature range experienced by a float over the lifetime in our data set was 12.44 °C. Method 2 produces more total corrections than method 1 (758 vs. 634), but method 1 produces a greater abundance of non-zero x_1 (dE_d/dT_s) (194 vs. 395). To visualize the cases of non-zero x_1, we display them separately (Figure 2). x_1 ranges from -3.4×10^{-5} to 2.3×10^{-5} (W m^{-2} nm^{-1} °C $^{-1}$) by method 2 compared to -2.4×10^{-5} to 1.2×10^{-5}

(W m^{-2} nm^{-1} °C $^{-1}$) by method 1 (Figure 1). Method 2's x_1 also shows greater variance with a larger standard deviation and interquartile range (Table 1). As such, method 1 produces a greater relative and absolute abundance of nonzero dE_d/dT_s and produces a more constrained dE_d/dT_s range than method 2. Values of the constant x_0 show, in general, a symmetric distribution around zero and of similar magnitude for all wavelengths (Figure 3).

Table 1. Nonzero x_1 by the night method and day method for all λ (W m^{-2} nm^{-1} °C^{-1} or µmol photons m^{-2}s^{-1} °C^{-1}), as shown in Figure 2.

Method	Median	IQR	Mean	SD
Night E_d	-6.7×10^{-6}	1×10^{-5}	-7×10^{-6}	8.5×10^{-6}
Day E_d	-5.8×10^{-6}	1.73×10^{-5}	-4.4×10^{-6}	1.3×10^{-5}
Night PAR	-1.064×10^{-2}	1.674×10^{-2}	-9.7×10^{-3}	1.31×10^{-2}
Day PAR	-9.53×10^{-3}	2.858×10^{-2}	9.6×10^{-3}	1.98×10^{-2}

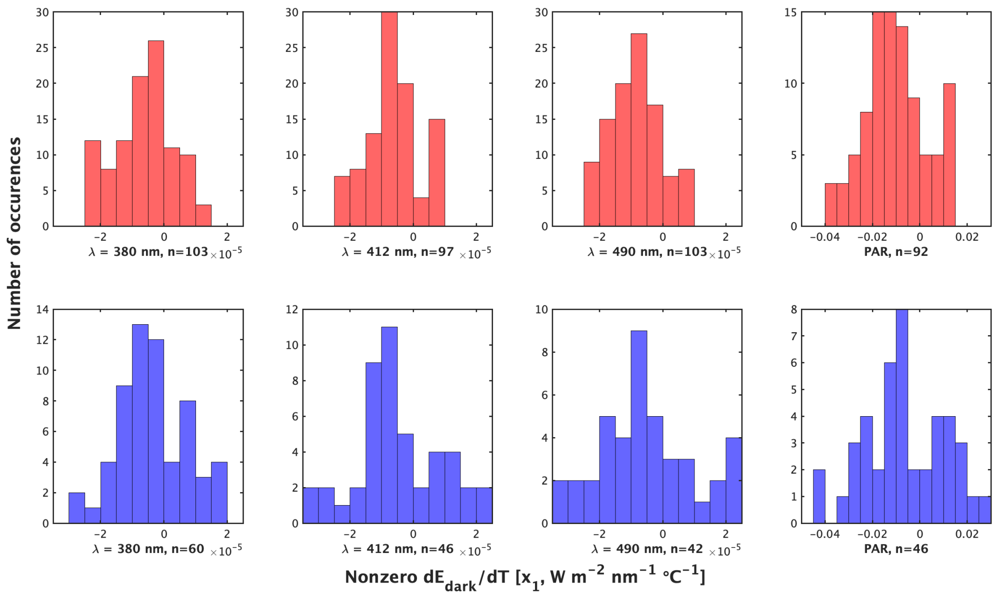

Figure 2. Histograms of the non-zero value of $x_1 = dE_d/dT_s$ (W m^{-2} nm^{-1} °C^{-1}) or $dPAR/dT_s$ (µmol photons m^{-2} s^{-1} °C^{-1}) by the night method (**top**) and day method (**bottom**) for (**left** to **right**) λ = 380 nm, 412 nm, 490 nm, and PAR.

Comparing the retrievals of x_1 for all floats that produced a correction by both methods, we find differences (Figure 4). For λ = 380 nm, 38 floats produced non-zero corrections for both methods, with a slope from robust regression = 1.12 and a Spearman's ρ = 0.75. At λ = 412 nm, 35 floats produced non-zero corrections for both methods, with a ρ = 0.90 and slope = 1.24, indicating an over-prediction at 412 nm by the day-time method. At λ = 490 nm, 31 floats produced both non-zero corrections, with a slope = 1.29 and ρ = 0.70. Combining all λ (n = 104) the slope is 1.15 and ρ = 0.79 (not shown). For PAR, there is a strong correlation between the methods with a slope = 1.03 and ρ = 0.85. Overall, this suggests for E_d a 15% overestimation by the day method compared to the night method, with λ-specific differences resulting in the largest overestimation by the night method compared to day at λ = 490 nm. However, at all λ and PAR, a Kolmogorov–Smirnov (k-s) test between the non-zero x_1 produced by both methods for the null acceptance results indicates the distributions are not different at the 5% significance level. Regressing x_0 values for all E_d (not shown) returns a slope = 1.04 with $\rho = 0.85$.

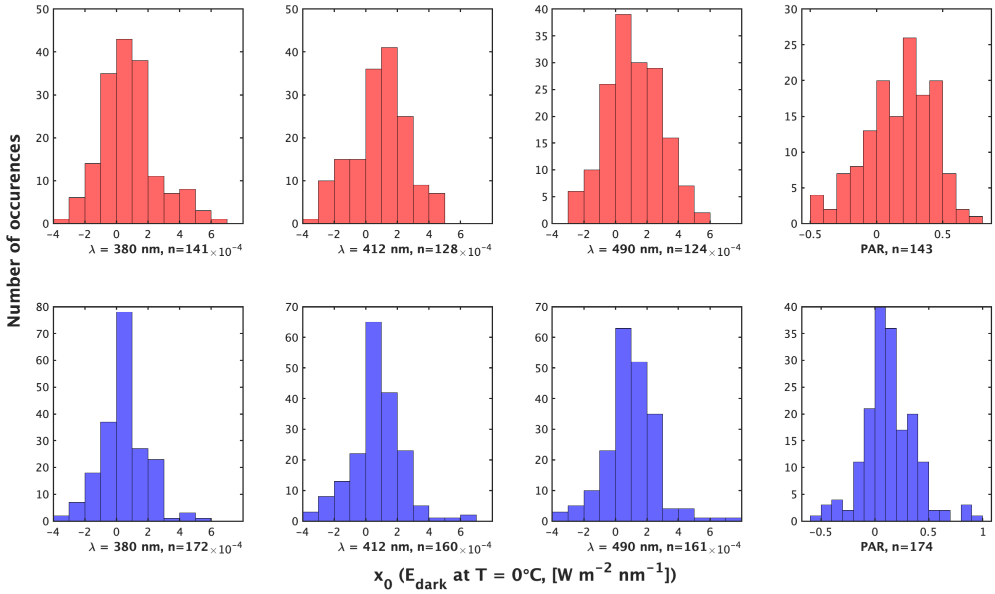

Figure 3. Histograms of the value of x_0 (W m^{-2} nm^{-1} or µmol photons m^{-2} s^{-1}) by the night method (**top**) and day method (**bottom**) for (**left** to **right**) λ = 380 nm, 412 nm, 490 nm and PAR. x_0 is the value reported by the irradiance sensor in the dark at T_s = 0 °C.

The correction is applied to each profile of a float as follows:

$$E_d(corrected) \ = \ E_d(measured) - [x_0 + x_1 \times T_s]. \tag{5}$$

Statistics on absolute size of corrections applied by methods 1 and 2 on good profiles at all λ (19,605,908 measurements corrected) highlight the smaller average correction with smaller variance by the night method compared to day, though the differences are small (Table 2, Figure 5). Both corrections provide similar and consistent results when applied to profile data (Figure 6, Table 3).

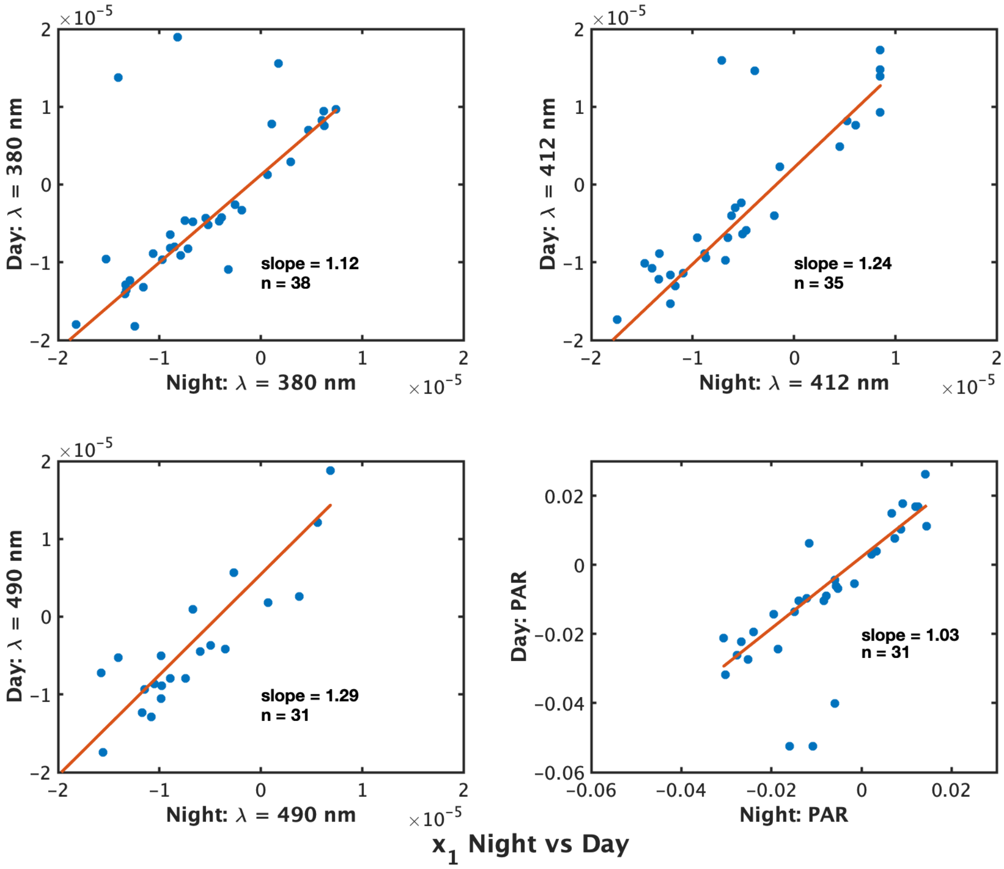

Figure 4. Comparison of x_1 obtained from nighttime profiles (x-axis) and daytime profiles (y-axis) (W m^{-2} nm^{-1} °C^{-1} or µmol photons m^{-2}s^{-1} °C^{-1}) for floats that produced non-zero x_1 using both methods. Results are presented for λ = 380 nm (**top left**), 412 nm (**top right**), 490 nm (**bottom left**), and PAR (**bottom right**).

Table 2. Absolute size of corrections applied by both methods on good profiles at all wavelengths and PAR (19,605,908 measurements corrected) (W m^{-2} nm^{-1} or µ mol photons m^{-2} s^{-1}).

Method	Max	Median	IQR	Mean	SD
Night E_d	4.44×10^{-4}	5.7×10^{-5}	9.3×10^{-5}	8.0×10^{-5}	7.2×10^{-5}
Day E_d	6.14×10^{-4}	7.1×10^{-5}	1.01×10^{-4}	9.3×10^{-5}	7.4×10^{-5}
Night PAR	5.52×10^{-1}	1.09×10^{-1}	2.3×10^{-1}	1.6×10^{-1}	1.41×10^{-1}
Day PAR	6.86×10^{-1}	1.4×10^{-1}	1.8×10^{-1}	1.72×10^{-1}	1.31×10^{-1}

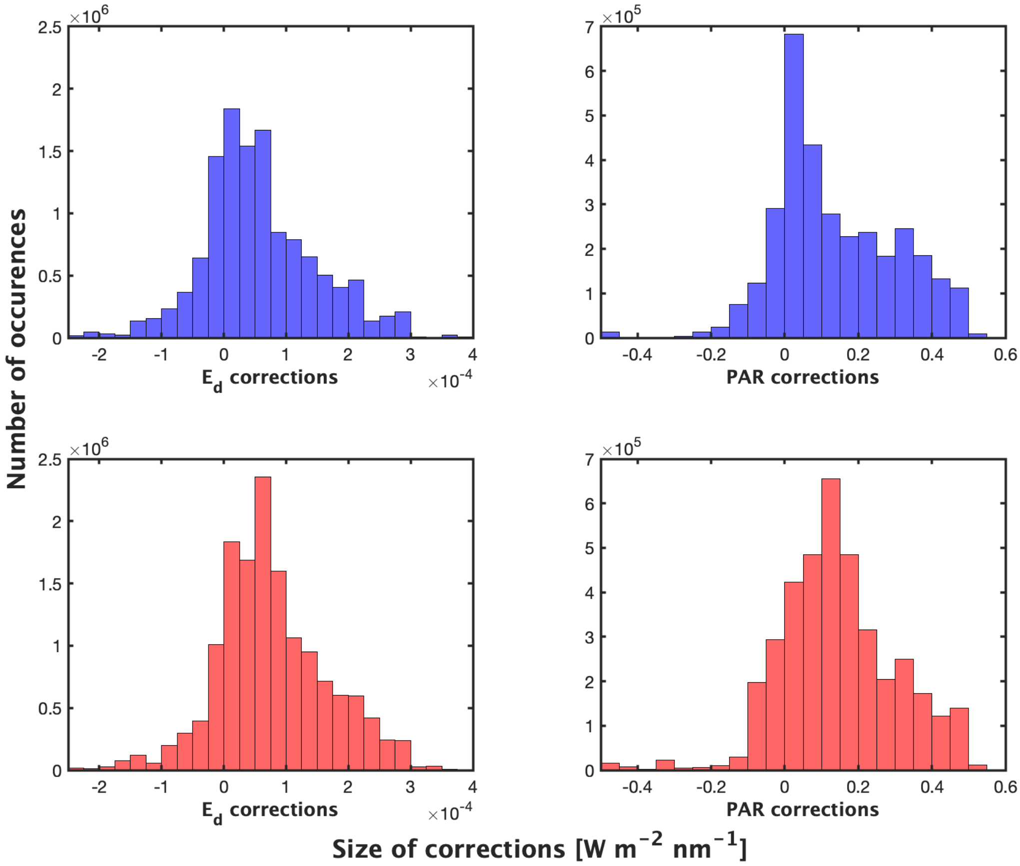

Figure 5. Size of corrections applied by the night (**top**) and day (**bottom**) method on good profiles at all wavelengths (19,605,908 measurements corrected) (W m^{-2} nm^{-1} or µmol photons m^{-2}s^{-1}). Statistics shown in Table 2.

Table 3. Measurements for all λ of measured $E_d(\lambda, z) < 0.01$ W m^{-2} nm^{-1} and PAR(z) < 1 µmol photons m^{-2} s^{-1}, corrected by the night and day methods (n = 12,930,490), as shown in Figure 6.

Method	Median	IQR	Mean	SD
Measured E_d	1.66×10^{-4}	5.76×10^{-4}	9.05×10^{-4}	1.82×10^{-3}
Night corrected E_d	4.8×10^{-4}	5.12×10^{-4}	8.2×10^{-4}	1.82×10^{-3}
Day corrected E_d	3.5×10^{-4}	5.05×10^{-4}	8.2×10^{-4}	1.83×10^{-3}
Measured PAR	2.65×10^{-1}	3.24×10^{-1}	3.18×10^{-1}	2.48×10^{-1}
Night corrected PAR	5.03×10^{-2}	1.77×10^{-1}	1.37×10^{-1}	2.09×10^{-1}
Day corrected PAR	3.9×10^{-2}	1.78×10^{-1}	1.13×10^{-1}	2.09×10^{-1}

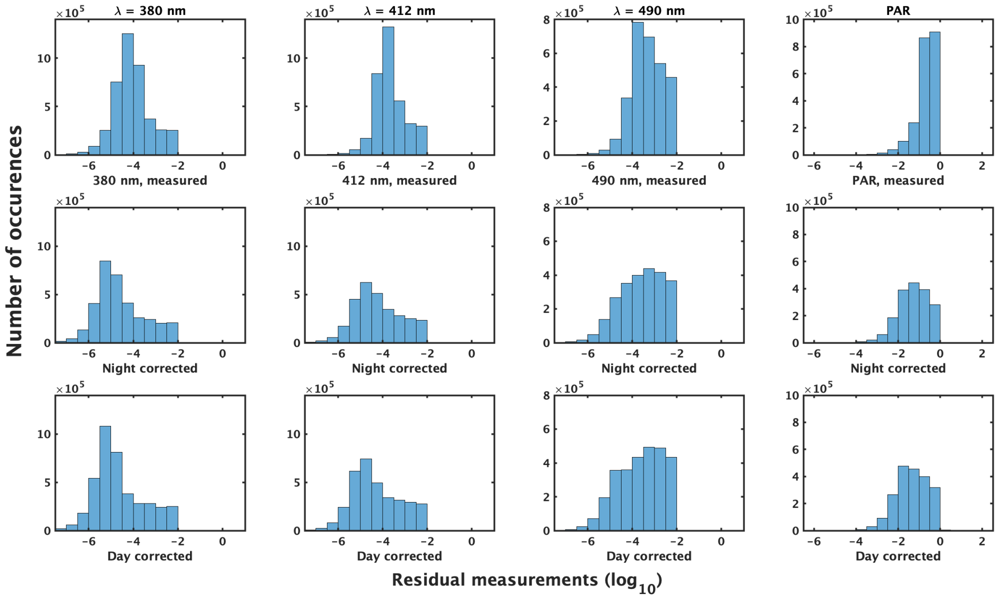

Figure 6. Measurements of $E_d(\lambda, z) < 1$ W m^{-2} nm^{-1} and PAR(z) < 100 µmol photons m^{-2} s^{-1} (**top** row) after corrections are applied by the night method (**middle** row) and day (**bottom** row). Columns are (**left** to **right**) λ = 380, 412, 490 nm and PAR. Plotted on log_{10} scale.

4. Discussion and Summary

For this BGC-Argo dataset, the mean absolute temperature corrections on E_d using night and day profiles are 8×10^{-5} and 9.3×10^{-5} [W m^{-2} nm^{-1}] and maximum absolute corrections are 4.4×10^{-4} and 6.14×10^{-4} [W m^{-2} nm^{-1}], respectively (Table 2). These corrections are more than an order of magnitude larger than the known sensitivity of the sensors (2.5×10^{-5} W m^{-2} nm^{-1}), are consistent with what has been observed in the lab by [4], and hence are significant. The average correction is O (10%) of the 0.1% light level, while the maximum is O (40%) of that value.

We further investigated whether the corrections had a significant impact on the diffuse attenuation coefficient:

$$K_d = -\frac{1}{E_d(z)}\frac{dE_d}{dz}, \tag{6}$$

for profiles corrected with both methods using a center difference scheme. While we observe differences (Table 4), they are small (on the order of 0.001 m^{-1}).

Table 4. K_d[m^{-1}] calculated on good daytime profiles, all λ, for measurements where $0.1 \leq E_d(\text{measured}) \leq 1$ (W m^{-2} nm^{-1}) (n = 1,741,267).

Method	Median	IQR	Mean	SD
Measured	0.052	0.013	0.053	0.035
Night corrected	0.051	0.013	0.053	0.034
Day corrected	0.05	0.014	0.051	0.031

Thus, the correction does not produce a significant impact on K_d at depth. As the temperature at depths is relatively constant, the impact of its gradient on K_d is small (<4%). The measured values of K_d are consistent with expected values for very clear waters, though higher than observed in the very clear waters of the Sargasso Sea [10,11].

The temperature correction for E_d is likely to prove most important in studies investigating light fields in the twilight zone and the impacts of radiance on deep organisms, such as [12]. Additionally, it will impact investigations into the minimum light level supporting phytoplankton growth and on the impact of night time illumination on biology. Organisms in these conditions are extremely sensitive to low ambient light. Understanding their reaction to light requires accurate measurements at low irradiance conditions.

The method used here follows the work of [4], who has demonstrated the temperature dependence of the dark current of Satlantic OCR504 radiometers in the laboratory. Additionally, ref. [5] published a method approaching the same goals as ours, i.e., to produce a temperature-dependent dark correction for BGC-Argo profiles. Though our methods differ, we find overall agreement with both [4,5]. Here we provide a simple and robust method that allow users to carry out their own corrections and is consistent with both [4,5]. In [5], the BGC-Argo B- and transmission files are used in addition to BGC-Argo s-files, while ours is based only on s-files. The B- and transmission files are used to investigate measurements made at float park depth, while the s-files contain compiled profiles for each float. Ref. [5] investigated 55 floats. They provide a model that includes drift correction, where in certain, but rare, cases they observed a drift as much as 1×10^{-7} $days^{-1}$, producing a significant correction over a 3 year lifetime. We found no significant evidence for this over the lifetime of the floats we analyzed. We recognize that by not investigating the measurements made at parking depth (instead basing our conclusion off of measurements made at deep profiles, where measurements may occasionally be as deep as ∼900 m), we are not using the best possible data to quantify a drift over the lifetime. The correction we have proposed did not take that into account. After the drift correction, they fit a linear model to provide a temperature correction analogous to our Equation (1). In [4], 7 radiometers were tested in the laboratory over a temperature range of 26 °C. They employed several methods for modeling the dark response: linear (such as ours), exponential, and quadratic. They chose the linear model as the primary model and only employed the quadratic or exponential if the R^2 value was significantly better. Out of 28 channels (7 radiometers × 4 channels), 17/28 were fit with the linear model, 4 with the exponential model, and 3 with the quadratic model, and for 4, no model fit well (Table 2a–g in [4]). The dynamic temperature range of their experiment compared to our in situ data (where average temperature range of a float lifetime is 12 °C) may explain the necessity for a quadratic fit compared to our data (e.g., Figure 8 in [4]). The values of our modeled coefficients dE_{dark}/dT agree well with [4] and [5], with the maximum dE_{dark}/dT on the order of $2-4 \times 10^{-5}$ W m^{-2} nm^{-1} °C^{-1} (Figure S9 in [5]). At all wavelengths and PAR, dE_{dark}/dT is centered near zero, slightly biased towards negative values (decreasing dark signal with increasing temperature), and assumes a general Gaussian form. For $dPAR_{dark}/dT$, ref. [4] produces the smallest values, on the order of 2×10^{-2} µmol photons m^{-2} s^{-1} °C^{-1}, while [5] agrees with our maximums as high as 4×10^{-2} µmol photons m^{-2} s^{-1} °C^{-1}. Likewise, we find a similar model constant of PAR (our x_0), with [5] showing the highest maximum. Our investigation of the daytime profiles revealed these significant dark readings at depth, and our corrections for PAR are of the same order relative to surface values as our corrections for E_d: at 10 m, our average PAR correction is on the order of 0.001% of the 10 m measured PAR value, analogous to the average 10 m correction at all three wavelengths. Overall we find very similar results between our method and [4,5]. The end-user applicability, robust approach, consistency between day and night methods (as in Figure 4), consistency between size of corrections applied across all four wavebands, and number of floats investigated here (219) provide evidence for the utility of the methods presented in this paper.

Based on the data presented here and elsewhere [4,5], we recommend that a correction for the temperature effect on the dark current be applied to all radiometry data on floats. When no nighttime profiles are available, a correction based on daytime measurements is better than no correction (as it is highly correlated with the nighttime correction, when both are available). However, it is best if sufficient nighttime profiles are available, as the correction made with them seems superior (more consistent between sensors and lower over all). This is sensible given the larger dynamic range in temperature that it is based on. Expanding profiles of radiance to greater depths is likely to also improve the correction.

Author Contributions: Conceptualization, E.B.; Methodology, E.B. and T.O.; Software, T.O.; Original draft preparation, T.O.; writing—review and editing, T.O. and E.B. All authors have read and agreed to the published version of the manuscript.

Funding: This research was funded by the National Aeronautics and Space Administration Ocean Biology and Biogeochemistry program grant number 80NSSC19K0001.

Data Availability Statement: All data used in this study come from a public data base: https://erddap.ifremer.fr/erddap/tabledap/ArgoFloats.html (accessed on 28 March 2022). Scripts to perform the methods in Matlab are available at https://github.com/TOceans/ArgoRadiometryDark (accessed on 28 March 2022).

Acknowledgments: We would like to express our deep gratitude to Herve Claustre from LOV and his team, who are responsible for the majority of the floats whose data are analyzed here and whose vision and determination resulted in radiometry being measured on the BGC-Argo floats. These data were collected and made freely available by the International Argo Program and the national programs that contribute to it. (https://argo.ucsd.edu (accessed on 28 March 2022), https://www.ocean-ops.org (accessed on 28 March 2022)). The Argo Program is part of the Global Ocean Observing System. We thank Andrew Thomas for help editing this manuscript. Comments by three reviewers helped improve this paper.

Conflicts of Interest: The authors declare no conflict of interest.

Appendix A. Solution to the Sensor Temperature Differential Equation

The partial differential equation

$$\frac{dT_s}{dt} = -\frac{T_s - T_{env}}{k}$$

whose solution (Equation (4) in the text) is derived as follows; We first solve the Homogeneous solution:

$$\begin{aligned}
\frac{dT_s}{dt} &= -\frac{T_s}{k} \\
dT_s\frac{1}{T_s} &= -\frac{1}{k}dt \\
\int dT_s\frac{1}{T_s} &= \int -\frac{1}{k}dt \\
ln(T_s) &= -\frac{t}{k} + C \\
T_s &= e^{-\frac{t}{k}+C} = Ae^{-\frac{t}{k}} \\
T_s(0) &= T_{env}(0) \text{ so } A = T_{env}(0)
\end{aligned}$$

The general solution is:

$$T_s = T_{env}(0)e^{-\frac{t}{k}}$$

For particular solution: Rewrite $\frac{dT_s}{dt} + \frac{T_s}{k} = \frac{T_{env}}{k}$ in standard form $y'(t) + p(t)y(t) = g(t)$, where $y = T_s$, $g = T_{env}$, and $p = \frac{1}{k}$. Then,

$$\begin{aligned}
y' &= pg - py \\
y' + py &= pg \\
\text{Introduce integration factor } \mu &= e^{\frac{t}{k}} = \frac{\mu'}{\mu} = p \\
\mu y' + \mu pg &= \mu pg \\
\mu py &= \mu' y \text{ by definition} \\
\mu y' + \mu' y &= \mu pg
\end{aligned}$$

$$\mu y' + \mu' y = (\mu y)'$$
$$(\mu y)' = \mu p g$$
$$\int (\mu y)' = \int \mu p g$$
$$\mu y = \int \mu p g$$
$$y = \frac{1}{\mu} \int \mu p g$$

$$\text{thus } T_s(t) = e^{-\frac{t}{k}} \int \frac{e^{\frac{t}{k}} T_{env}(t)}{k} dt$$

Solution = general solution + specific solution:

$$T_s(t) = T_{env}(0) exp(\frac{-t}{k}) + exp(\frac{-t}{k}) \int_{t'=0}^{t'} \frac{exp(\frac{t'}{k}) \times T_{env}(t')}{k} dt.$$

References

1. Xing, X.; Morel, A.; Claustre, H.; Antoine, D.; D'Ortenzio, F.; Poteau, A.; Mignot, A. Combined processing and mutual interpretation of radiometry and fluorimetry from autonomous profiling Bio-Argo floats: Chlorophyll a retrieval. *J. Geophys. Res.* **2011**, *116*, C06020. [CrossRef]
2. Xing, X.; Morel, A.; Claustre, H.; d'Ortenzio, F.; Poteau, A. Combined processing and mutual interpretation of radiometry and fluorometry from autonomous profiling Bio-Argo floats: 2. Colored dissolved organic matter absorption retrieval: CDOM absorption retrieval from Bio-Argo. *J. Geophys. Res. Ocean.* **2012**, *117*, C04022. [CrossRef]
3. Roemmich, D.; Alford, M.H.; Claustre, H.; Johnson, K.; King, B.; Moum, J.; Oke, P.; Owens, W.B.; Pouliquen, S.; Purkey, S.; et al. On the Future of Argo: A Global, Full-Depth, Multi-Disciplinary Array. *Front. Mar. Sci.* **2019**, *6*, 439. [CrossRef]
4. Xing, X.; Lagunas-Morales, J. Laboratory results on the dependence of dark current upon environmental temperature variability for Satlantic's OCR504 radiometers. In *Optical Precision Manufacturing, Testing, and Applications*; Proc. SPIE 10847: Beijing, China, 2018; p. 11. [CrossRef]
5. Jutard, Q.; Organelli, E.; Briggs, N.; Xing, X.; Schmechtig, C.; Boss, E.; Poteau, A.; Leymarie, E.; Cornec, M.; D'Ortenzio, F.; et al. Correction of Biogeochemical-Argo Radiometry for Sensor Temperature-Dependence and Drift: Protocols for a Delayed-Mode Quality Control. *Sensors* **2021**, *21*, 6217. [CrossRef]
6. Cullen, J.J.; Davis, R.F. The Blank Can Make a Big Difference in Oceanographic Measurements. *Limnol. Oceanogr. Bull.* **2003**, *12*, 29–35. [CrossRef]
7. Organelli, E.; Claustre, H.; Bricaud, A.; Barbieux, M.; Uitz, J.; d'Ortenzio, F.; Dall'Olmo, G. Bio-optical anomalies in the world's oceans: An investigation on the diffuse attenuation coefficients for downward irradiance derived from Biogeochemical Argo float measurements: World's ocean bio-optical anomalies. *J. Geophys. Res. Ocean.* **2017**, *122*, 3543–3564. [CrossRef]
8. Koblick, D. Vectorized Solar Azimuth and Elevation Estimation. MATLAB Central File Exchange. 2021. Available online: https://www.mathworks.com/matlabcentral/fileexchange/23051-vectorized-solar-azimuth-and-elevation-estimation (accessed on 26 July 2021).
9. Bittig, H.C.; Maurer, T.L.; Plant, J.N.; Schmechtig, C.; Wong, A.P.S.; Claustre, H.; Trull, T.W.; Udaya Bhaskar, T.V.S.; Boss, E.; Dall'Olmo, G.; et al. A BGC-Argo Guide: Planning, Deployment, Data Handling and Usage. *Front. Mar. Sci.* **2019**, *6*, 502. [CrossRef]
10. Lee, Z.; Wei, J.; Voss, K.; Lewis, M.; Bricaud, A.; Huot, Y. Hyperspectral absorption coefficient of "pure" seawater in the range of 350–550 nm inverted from remote sensing reflectance. *Appl. Opt.* **2015**, *54*, 546. [CrossRef]
11. Smith, R.C.; Baker, K.S. Optical properties of the clearest natural waters (200–800 nm). *Appl. Opt.* **1981**, *20*, 177. [CrossRef] [PubMed]
12. Om, M.M.; Steinberg, D.K.; Stamieszkin, K. Cloud shadows drive vertical migrations of deep-dwelling marine life. *Proc. Natl. Acad. Sci. USA* **2021**, *118*, e2022977118. [CrossRef] [PubMed]